

Observation on Physical Growth of Nonmetallic Inclusion in Liquid Steel During Ladle Treatment

YOUNGJO KANG, BAHMAN SAHEBKAR, PIOTR R. SCHELLER, KAZUKI MORITA, and DU SICHEN

The behaviors of several types of inclusions at a high temperature were examined using a confocal scanning laser microscope (CSLM, 1LM21H/SVF17SP). Although alumina inclusions tended to impact on each other, agglomerate, and grow quickly, no other inclusion type, such as spinel as well as solid and liquid calcium aluminate, was observed to attract each other. The results of confocal microscope study were compared with the industrial investigation. For this purpose, many steel samples were taken at different stages of ladle treatment. The samples were analyzed by scanning and light optical microscopes. Approximately 50,000 inclusions of several types were examined. Only alumina inclusions were attracted to each other and agglomerate. No agglomeration by attractive behavior was observed in the other types of inclusions, including liquid inclusions. Both the industrial data and the *in situ* observation by CSLM indicate that, although the attraction force and the agglomeration play a significant role in the growth of alumina inclusions, the agglomeration of spinel and calcium aluminate inclusions does not need special consideration in ladle treatment. The agglomeration of liquid calcium aluminate inclusions took place only when they occasionally met as a result of external force, which led to low collision probability. However, the agglomeration of the liquid calcium aluminate inclusions along with alumina particles could be detrimental in the casting process.

DOI: 10.1007/s11663-011-9497-2

© The Minerals, Metals & Materials Society and ASM International 2011

I. INTRODUCTION

NONMETALLIC inclusions, in most cases, detrimentally affect the quality of the final steel product. In the last decades, great efforts have been made to reduce the number of inclusions in the steel. Bigger nonmetallic inclusions would have a better probability of being removed to the slag phase by buoyancy force. However, inclusions that have larger sizes are more harmful when they remain in the final product. To optimize the steelmaking processes, knowledge of physical growth of the inclusions resulting from agglomeration is essential. In line with this direction, several studies^[1–8] have been carried out to study and model the agglomeration of inclusions. However, understanding of the physical growth of inclusions in liquid steel is still limited.

In a pioneer work, Emi introduced a confocal scanning laser microscope (CSLM) in steel research.^[9–12] The device detects blur-free signals only from the focal plane. The combination of a microscope with a laser enables

high-resolution images at high temperature. Since then, many phenomena of nonmetallic inclusions in iron- and steelmaking, such as dissolution,^[13–16] precipitation, and crystal growth,^[17–20] have been examined *in situ*. Although observations have been made of the behavior of the inclusions in liquid steel,^[21,22] most studies have been focused on the slag–metal interface. Yin *et al.*^[23,24] employed this technique to study the agglomeration and growth of inclusions on the surface of liquid steel. Despite these valuable investigations, little has been done to compare the observation in the confocal microscope with the findings in industrial practice. It is noted that the behaviors of inclusions observed in the confocal microscope is related to their movement on the steel surface. Whether they would behave similarly in the bulk of liquid steel has been an important but unclear issue for researchers and industrial engineers.

The present research aims at the industrial investigation of the inclusions in ladle treatment as well as a laboratory study of the behavior of the inclusions using a confocal microscope. It is expected that a comparison of the results of these two types of studies would provide a clear idea regarding the physical behavior of different types of inclusions in the bulk of liquid steel.

II. EXPERIMENTAL

A. Industrial Study

To study the behaviors of inclusions in liquid steel, steel samples were taken during ladle treatment in

YOUNGJO KANG, formerly with the Institute of Industrial Science, The University of Tokyo, Tokyo 153-8505, Japan, is now Senior Researcher with Technical Research Laboratories, POSCO, Pohang, Korea. BAHMAN SAHEBKAR, Former Senior Engineer, and PIOTR R. SCHELLER, Professor, are with the Institute of Iron and Steel Technology, Freiberg University of Mining and Technology, Freiberg 09596, Germany. KAZUKI MORITA, Professor, is with the Institute of Industrial Science, The University of Tokyo, Tokyo 153-8505, Japan. DU SICHEN, Professor, is with the Department of Materials Science and Engineering, Royal Institute of Technology, Stockholm 100 44, Sweden. Contact e-mail: du@mse.kth.se

Manuscript submitted September 15, 2010.

Article published online March 4, 2011.

Table I. Typical Chemical Compositions of Steel ORVAR 2M

Element	C	Si	Mn	Cr	Mo	V
Wt pct	0.39	1.0	0.4	5.3	1.3	0.9

Uddeholm Tooling AB (Hagfors, Sweden). In most experiments, the steel grade ORVAR 2M, (the representative composition is shown in Table I), was studied. The inclusions in the samples were analyzed carefully. The process in Uddeholm Tooling AB was described in detail in an earlier work.^[25] Liquid crude steel melted in an electric arc furnace (EAF) from scrap metal is tapped into a ladle. After removing the EAF slag, Al deoxidation, addition of slag former, and alloying are carried out. The ladle is then transferred to a degassing station, where the closed chamber is evacuated to 300 Pa. Meanwhile, the ladle is stirred by both gas and induction. Once the target steel composition is met, the liquid metal is sent for casting.

Steel samples were taken at different stages, namely, (1) after deslagging (EAF slag), (2) before vacuum treatment, (3) after vacuum treatment, and (4) before casting. A rapid solidification method was employed to take steel samples. A strong argon stream was flown from the tip of a sampler to keep molten slag from being entrapped. When the sampler reaches the steel melt, the interior of the sampler was evacuated to suck in the steel. Each sample was in the shape of a lollipop and was quenched in water and prepared for the inclusion analysis. In total, 18 heats were studied. Well-polished samples were examined using a light optical microscope (LOM) to study the sizes and shapes of inclusions. The compositions of the phases in the inclusions were identified manually using a JSM-840 scanning electron microscope (SEM, JEOL, Tokyo, Japan) equipped with an energy-dispersive X-ray analyzer (EDX, INCAEnergy, Oxford, U.K.).

B. CSLM Study

1. Experimental setup

To examine the behaviors of inclusions at the surface of liquid steel, a CSLM (1LM21H/SVF17SP; Lasertec, Naples, FL) was employed. A gold-coated, high-temperature furnace is equipped with the CSLM as illustrated in Figure 1. The furnace is tightly sealed with o-rings to ensure atmosphere control. A rotary vacuum pump is attached to evacuate the chamber to 1 Pa. The pressure in the chamber is controlled by a pressure sensor. An observation quartz window ($\phi 0.008$ m) on the top enables examination of the sample by microscope. In the chamber, a halogen lamp is installed at the bottom. Cooling air protects the lamp from overheating breakage. An elliptical shape and gold coating allow for most reflected beams from the lamp to focus on the upper focal point, where a sample is placed. It is possible to heat the sample to 1973 K (1700 °C) by radiation. The sample usually is held in a sample holder, which consists of a platinum plate, an alumina tube, and Pt-6

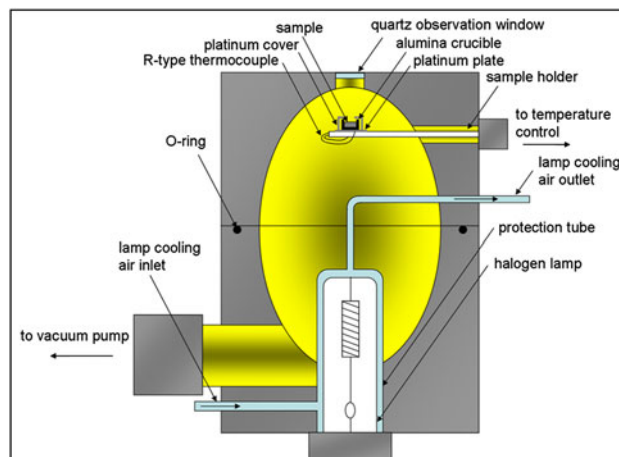


Fig. 1—Illustration of high-temperature chamber of a CSLM.

pct Rh/Pt-30 pct Rh thermocouple. The whole furnace unit is cooled by flowing water. In the CSLM, a He-Ne or a semiconductor laser is used for observation. The obtained image could be watched using a cathode ray tube (CRT) monitor and recorded onto a video tape.

2. Sample preparation and observation procedures

Steel samples taken before vacuum treatment at Uddeholm Tooling were used in the CSLM. In this type of sample, spinel inclusions often were found. A steel sample was cut into the dimension and placed in an alumina crucible that has an inner diameter of 9 mm and an inner height of 4 mm. The sample on the sample holder was covered by a platinum lid with an opening on the top for observation, which enables thermal homogeneity in the system.

In a part of the experiments attempting to observe liquid inclusions, synthetic inclusions were introduced along with the steel sample because of the limited condition for the formation of liquid inclusions. Regent grade Al_2O_3 and CaO calcined from CaCO_3 at 1273 K (1000 °C) for 24 hours were weighed and mixed in mortar aiming the composition of $12\text{CaO } 7\text{Al}_2\text{O}_3$. The oxide mixture held in a platinum crucible was premelted at 1773 K (1500 °C) for 1 hour to obtain a homogeneous melt. It was crushed and screened under $38 \mu\text{m}$ to obtain synthetic calcium aluminate “liquid” inclusions. The fine calcium aluminate particles additionally were mixed with powdery electrolytic iron (99.9 pct $-150 \mu\text{m}$) in the mass ratio approximately 1:1000. The reason for using this mass ratio was to prevent the synthetic inclusion particles from attaching and growing before observation. Preliminary experimental results indicated that this was a good ratio. The mixture was placed between two pure iron disks (99.5 pct, $\phi 8$ mm) in the alumina crucible. It should be mentioned that many solid alumina inclusions were found in the iron disks employed. Hence, the sample would contain both liquid calcium aluminate inclusions and solid alumina inclusions at the experimental temperature (1873 K [1600 °C]).

After the sample was placed in the sample holder, the chamber was sealed tightly. The chamber was evacuated to 1 Pa before argon gas ($\text{O}_2 < 2\text{ppm}$) was introduced.

The evacuation and argon-filling procedure was repeated at least five times to flush out the oxygen completely. To obtain an even lower oxygen partial pressure, gas mixtures of argon and hydrogen were employed in some experiments. The volume percents of the mixture gases were Ar + 1 vol pct H₂, + 2 vol pct H₂, and + 3 vol pct H₂. The oxygen content in liquid steel by the atmosphere control will be in the range of 1 to 500 ppm. Although the influence of the oxygen content on the surface tension of liquid steel is obviously large, the variation of the surface tension was expected to be 1.4 to 2.0 N/m, which could be regarded as relatively insignificant in the present study.

The laser microscope was focused on the surface of the sample. Thereafter, the sample is heated to 1923 K (1650 °C) at a heating rate of 1 K/s. After 5 minutes for homogeneity, the sample temperature is reduced to 1873 K (1600 °C). It should be mentioned that the real temperature of the sample is somewhat lower than the indicated value. The difference was estimated to be about 30 K (30 °C) by melting pure substances the melting points of which are well known. The image of the surface was examined and recorded by the CRT monitor and the video recorder. Still frames were taken from the recorded movie clip with a time step of 0.5 seconds and were carefully analyzed.

After the experiments in the CSLM, the inclusions observed were identified by a SEM (LEO 430; Leo Electron Microscopy, Cambridge, U.K.) with an EDX analyzer (Röntec, Berlin, Germany), and an electron probe microanalyzer (JXA-8800, JEOL)

III. RESULTS AND DISCUSSION

A. Inclusions Found in the Industrial Samples

An earlier study^[26] at Uddeholm Tooling AB revealed eight types of inclusions during ladle treatment. In the present work, six of the eight types were detected. The results are summarized in Table II where the notations of the previous study are adopted to maintain consistency.

At the early stage of ladle treatment, most inclusions were the spherical inclusions of type 2. It is a liquid oxide solution of Al₂O₃, CaO, MgO, and SiO₂ (The SiO₂ content could be as high as 15 mass pct). Type 2

inclusions were found throughout the ladle treatment, even before casting. Type 3 inclusions (spinel) and type 4 inclusions, which consist of both the spinel phase and the liquid phase in type 2, were found after deslagging. Both, however, disappeared after vacuum degassing. After Al deoxidation, another type of liquid oxide inclusions with low MgO and SiO₂ content, namely type 7, were detected. It also was found that some liquid inclusions with the type 7 composition bore pieces of spinel or MgO. The former is named type 6 and the latter type 8. An example of type 8 inclusions is presented in Figure 2, which shows the MgO island. The major difference between type 2 and type 7 is their SiO₂ contents. Type 2 has a SiO₂ content around 15 to 20 mass pct, whereas the SiO₂ content in type 7 is usually lower than 4 to 5 mass pct.

It should be mentioned that inclusions of type 1 (MgO) and type 5 (Al₂O₃) listed in Table II were not detected in the present work. As reported in the earlier study,^[25] type 1 inclusions were found only in the fresh ladle because of MgO dust, and the Al₂O₃ inclusions were found only during and shortly after aluminum addition.^[27] Because no samples were taken in the fresh ladle and during the aluminum addition, type 1 and type 5 inclusions were not detected.

The results of the industrial samples are presented in Table III. The total area of steel samples analyzed under

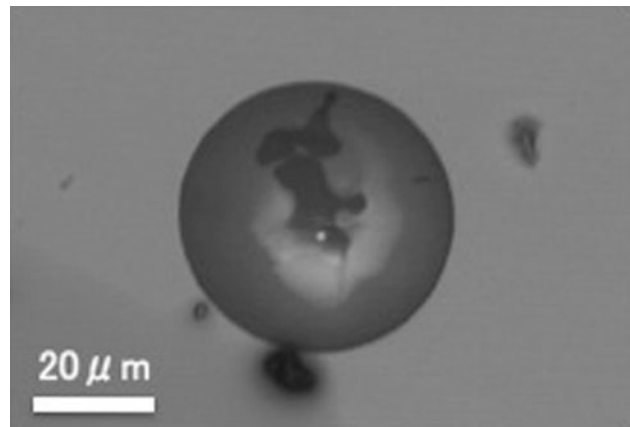


Fig. 2—Microphotograph of a typical liquid calcium aluminate inclusion bearing MgO island (type 8).

Table II. Presence of Various Types of Inclusions in Ladle Treatment

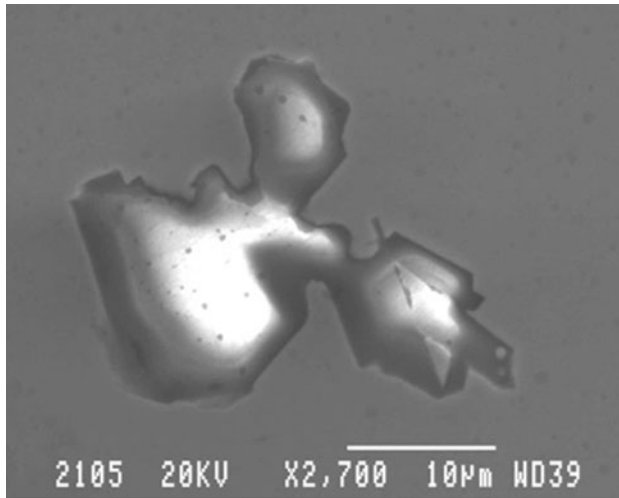
Type*	Description	After Deslagging	Before Vacuum	After Vacuum	Before Casting	Origin
1	pure MgO					refractory
2	liquid oxide solution with high SiO ₂	×	×	×	×	ladle glaze, EAF slag
3	spinel	×	×			
4	coexistence of 2 and 3	×	×			
5	pure Al ₂ O ₃					Al addition
6	coexistence of 7 and 3		×	×	×	ladle glaze
7	liquid oxide solution with low SiO ₂		×	×	×	
8	coexistence of 7 and 1 (in old ladle)			×	×	

*Referred after T. Nagendra.^[26]

Table III. Amount of Different Types of Inclusions Examined and Their Appearance Regarding Attachment and Agglomeration*

	Stages				Attachment	Agglomeration
	After Deslagging	Before Vacuum	After Vacuum	Total		
Analyzed area (mm ²)	6525	19,873	22,927	51,825		
Observed inclusions	4934	16,315	5956	29,265		
Type 2-based inclusions	65 pct	19 pct	11 pct		No	No
Spinel	35 pct	33 pct	—		No	No
Alumina	—	—	—		Yes	Yes
Type 7-based inclusions	—	48 pct	89 pct		No	No

*The numbers of steel samples is different at different stages in the table.

Fig. 3—Microphotograph of an alumina inclusion.^[22]

a LOM was more than 50,000 mm². Approximately 30,000 of nonmetallic inclusions were found and examined. The number of inclusions that could be identified was bigger than 0.5 μm. And most LOM observation was carried out using × 200 and × 500. The Swedish Standard (SS 11 11 16) was chosen to classify the observed inclusions in their size.

Because the spinel phase in type 4 is surrounded by the same liquid oxide solution phase found in type 2, the physical behaviors of these two types of inclusions with respect to agglomeration and growth could be expected to be similar. Similarly, the type 6 and 8 inclusions would have similar properties as in type 7 in the sense of agglomeration and growth. Hence, the total number (total percentage) of inclusions of types 2 and 4 are presented in one group and the total number of inclusions of types 6 through 8 are presented in another group. Despite the considerably large area and the large amount of inclusions examined, none of those examined in this study showed indications of attachment or agglomeration. However, alumina inclusions have been observed at the early stage of deoxidation in the ladle treatment at Uddeholm Tooling in the previous study.^[27] In contrast with the other types of inclusions, the alumina inclusions were found only in the form of clusters. Figure 3 shows a typical example of the

alumina clusters found during deoxidation. It should be mentioned that only a few alumina clusters were found, which was a result of the fast agglomeration and separation of alumina inclusions.^[27]

B. Behavior of Various Inclusions on Liquid–Steel Surface

CSLM observations of steel samples were conducted only in Ar, Ar + 1 vol pct H₂ and Ar + 2 vol pct H₂ as mentioned in the Section II.

The argon gas used in the present study had, at most, an oxygen level of 2 ppm. In addition to the oxygen in the argon gas, a certain amount of oxygen also would diffuse into the reaction chamber through the O-ring sealing. However, the steel samples from Uddeholm Tooling contained a high content of Al (about 0.07 mass pct). The “high” oxygen level along with the high Al content would lead to the formation of numerous Al₂O₃ inclusions. In fact, many inclusions were observed under the CSLM when Ar gas was employed. Postanalysis revealed that most inclusions were alumina.

The alumina inclusions collided frequently, and the collisions always resulted in agglomeration. A series of images in Figure 4 demonstrate the process of agglomeration of the alumina inclusions. It is clearly shown that several groups of inclusions collide and agglomerate within seconds. This observation is in accordance with previous studies.^[23,24]

It was also observed that the alumina inclusions often were attracted to each other. The attraction was sometimes present even between long distances. Figure 5 shows the trajectories of alumina inclusions on the liquid steel surface with the interval of 0.5 seconds between frames. Four inclusions were traced along the frames. It was also confirmed that all inclusions were alumina.

The collision between inclusions A and B and, consequently, their agglomeration took place in about 3 seconds. The moment when inclusion A floated up was regarded as $t = 0.0$. The initial distance between inclusions A and B was approximately 135 μm. From the next moment, inclusion B moves toward inclusion A, whereas inclusion A and other inclusions move in almost the same manner, which is probably caused by the surface movement. Inclusions A and B’s movement toward each other is strong evidence that the attractive

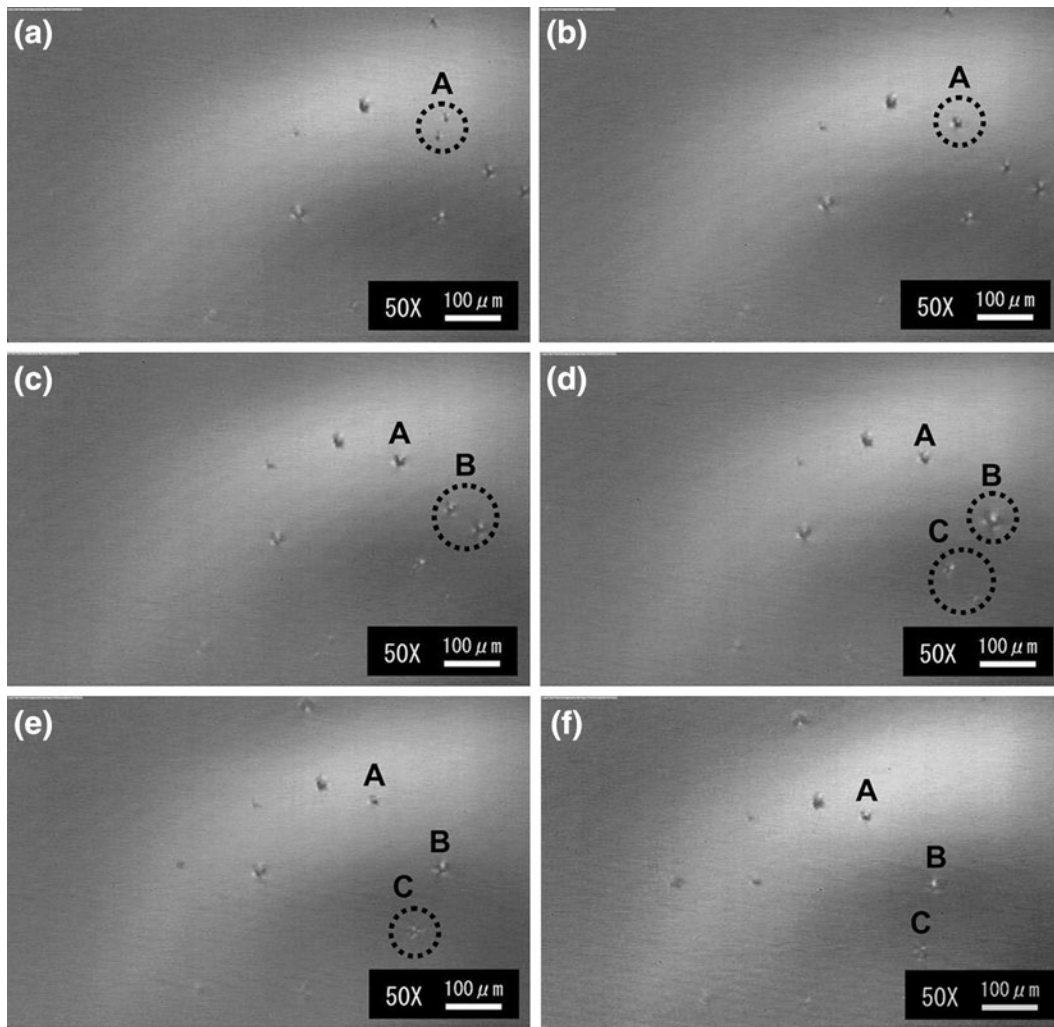


Fig. 4—Images from the CSLM, showing the agglomeration of alumina inclusions: (a) $t = 0.0$ s, (b) $t = 1.0$ s, (c) $t = 2.0$ s, (d) $t = 3.0$ s, (e) $t = 4.0$ s, and (f) $t = 5.0$ s.

interaction was applied between the two inclusions, which are located far apart. Immediately before the two inclusions begin agglomerating, the distance between them is estimated to be about $28 \mu\text{m}$. However, it also is observed that inclusions C and D maintain the interparticle distance less than $100 \mu\text{m}$ for about 3 seconds. To understand this discrepancy, the effect of the inclusion size may need to be considered.

The size of alumina inclusions would increase after the agglomeration. It is expected that the self-agglomeration greatly contributes to the growth of the alumina inclusion. As shown in Figure 6, the sizes of the alumina inclusions are in the order of $10 \mu\text{m}$ in the initial state (Figure 5(a)). However, many inclusions larger than $50 \mu\text{m}$ can be observed after only 60 seconds (Figure 5(b)).

The CSLM results show that alumina inclusions strongly attract each other and agglomerate readily. Consequently, the alumina inclusions grow quickly by agglomeration. In fact, the agglomeration behavior of the alumina inclusions has been reported by many researchers.^[1,3,23] Yin *et al.*^[23] also have observed

long-range attraction between alumina inclusions. These authors also have estimated the attraction force using particle mass and acceleration. It would be interesting to make a similar calculation to discover whether the attraction force resulting from the mass is a dominating factor in the attraction and agglomeration of the inclusions.

As a first approximation, an inclusion particle is assumed to be a sphere. The size of an inclusion is averaged from a few graphical measurements on the particle. Based on the diameter, the volume and mass of the inclusion were estimated. A geometric average of the masses of both particles was employed as the mass of the moving object. This average should be allowed as the size differences in the particles were small. From a series of frames, the velocity and acceleration of the moving object are evaluated. The attraction force is calculated using the product of the equivalent mass and acceleration. In Table IV, the ranges of measured diameter, calculated volume, mass, acceleration, and force are summarized for the alumina inclusions that have approached each other and then agglomerate.

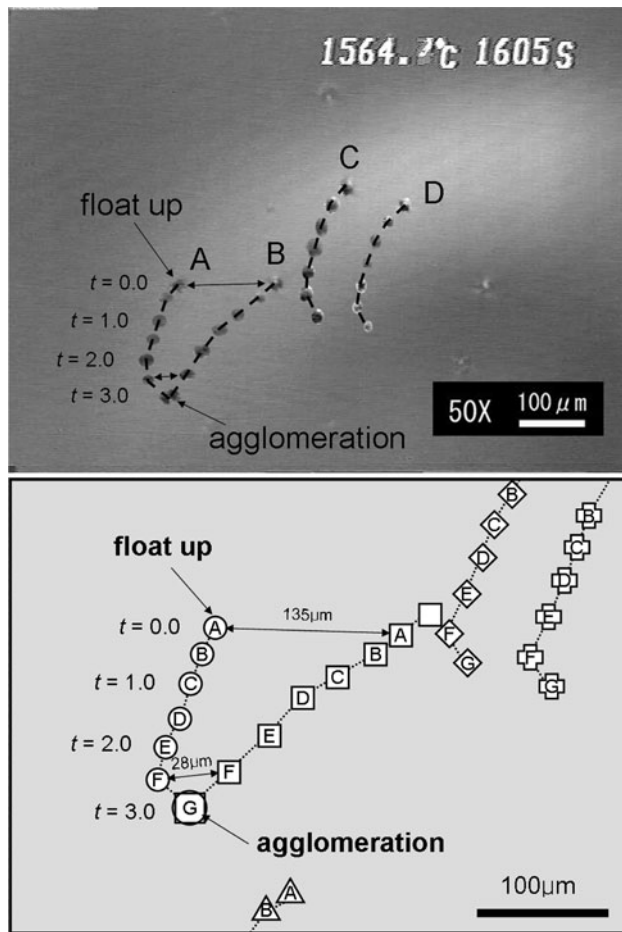


Fig. 5—Trajectories of a group of the alumina inclusions, showing self-attraction.

Note that the acceleration was determined by analyzing the change in the interparticle distance with time. The attractive force that results in approaching and agglomeration is in the order of 10^{-14} – 10^{-16} N. This range agrees well with the previous study.^[23]

When Ar + 1 vol pct H₂ gas mixture was used, alumina inclusion formation was limited. The population of inclusions observed under CSLM was lower than that when only Ar gas was used. According to SEM analysis carried out after the experiments, the inclusions found in the samples were mostly spinel inclusions. The spinel inclusions usually had sharp edges (solid), which were useful for identifying this type of inclusion during observation under CSLM. Most spinel inclusions were also smaller than 10 μm, and the size of the inclusions hardly increased with time. The inclusions were moving in almost the same direction along the surface flow. No collisions or attractions were observed.

Typical examples of the movements of the spinel inclusions on the surface are shown in Figure 7. When inclusion A initially was traveling in the left-upward direction, another inclusion (marked as B) floated to the surface (Figure 7(b)). When inclusion B floated to the top, the distance between the two inclusions was about 25 μm. Although this distance seemed to be short compared with the alumina inclusions, the two

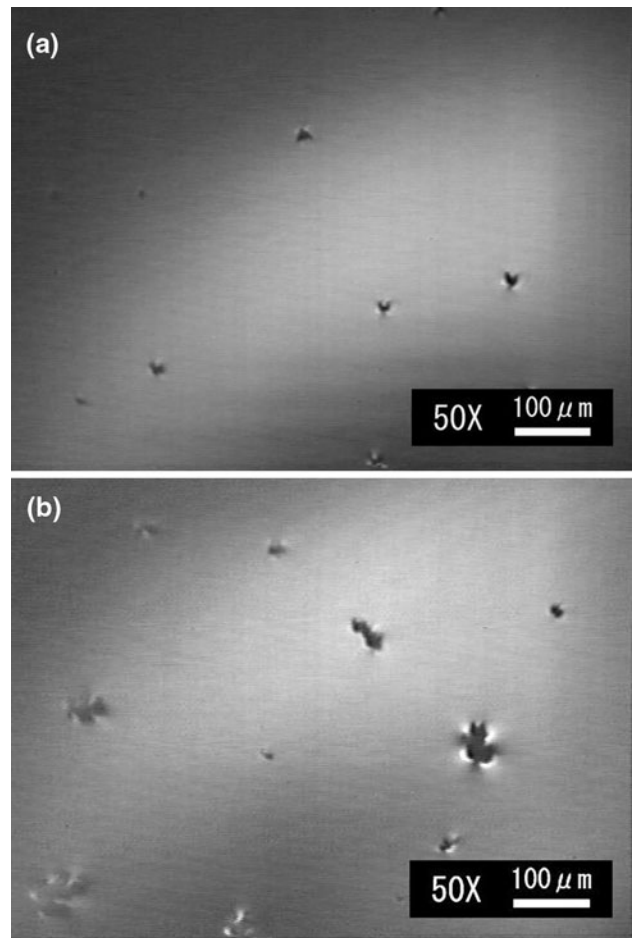


Fig. 6—Images from the CSLM, showing the growth of alumina inclusions, (a) before, $t = 0$ s; (b) after, $t = 60$ s.

Table IV. Estimated Force Range Applied to the Agglomerating Alumina Inclusions

Average diameter (m)	10^{-5} to 2×10^{-5}
Volume (m ³)	8×10^{-16} to 2×10^{-15}
Mass (kg)	10^{-11} to 5×10^{-11}
Acceleration (m s ⁻²)	2×10^{-4} to 10^{-5}
Attractive force (N)	10^{-14} to 10^{-16}

inclusions kept the distance constant for 4 seconds without attracting or getting closer.

The use of Ar + 2 pct H₂ gas mixture resulted in an even lower oxygen partial pressure. In this case, most observed inclusions were another kind of small solid inclusions. The SEM analysis revealed that the compositions of the inclusions were similar to CaO 2Al₂O₃; the liquidus temperature of which was around 2000 K (1727 °C). Most inclusions were in the size range between 10 μm and 20 μm. No agglomeration and consequently no growth in size were observed for this type of inclusion. This aspect is exemplified by the images in Figure 8. Figure 8(b) shows one calcium aluminate inclusion (inclusion B) that just floated up to the surface next to another (inclusion A). The distance

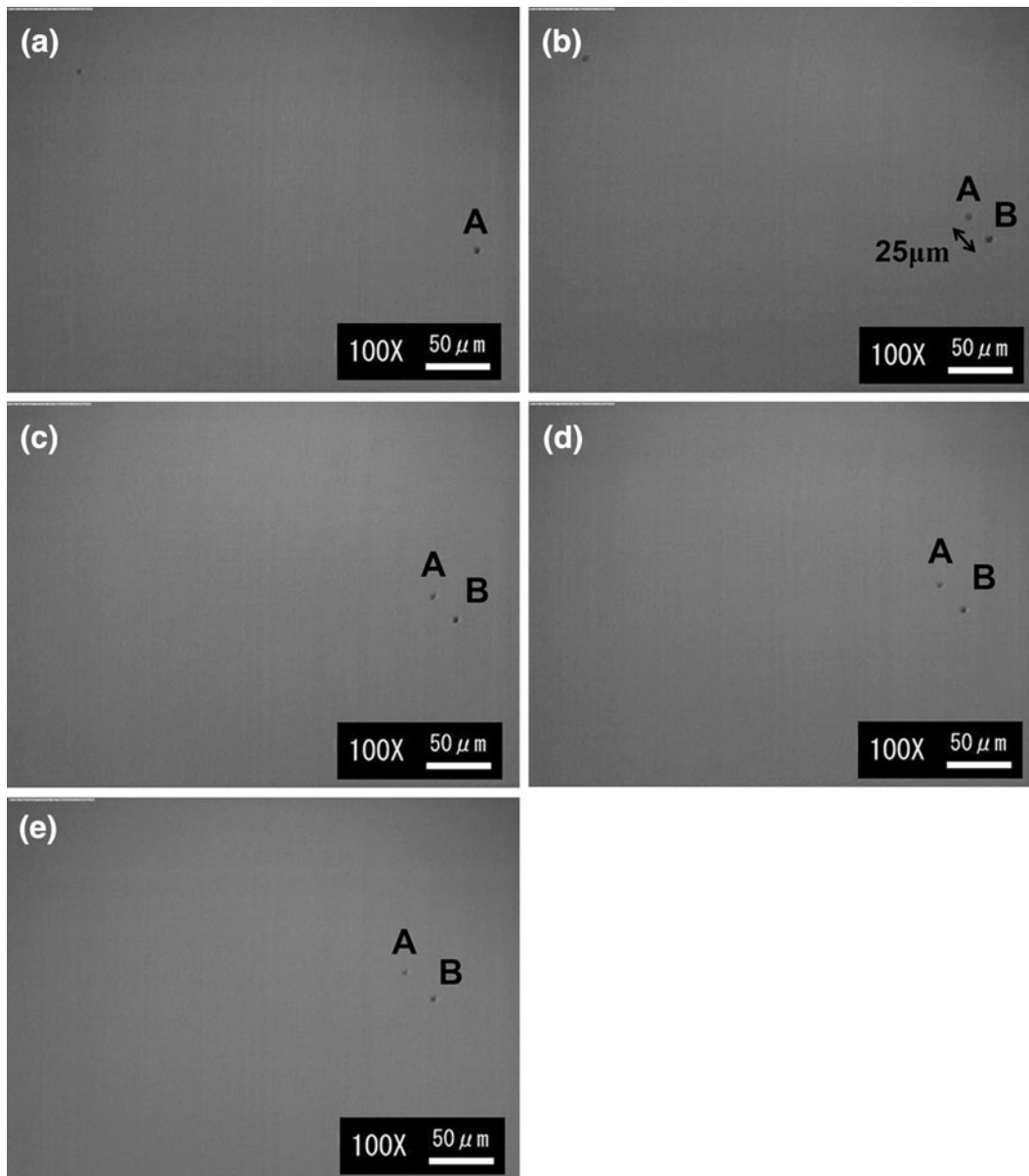


Fig. 7—Images from the CSLM, showing a pair of spinel inclusions keeping their distance from each other: (a) $t = 0.0$ s, (b) $t = 1.0$ s, (c) $t = 2.0$ s, (d) $t = 3.0$ s, (e) $t = 4.0$ s, and (f) $t = 5.0$ s.

between these two inclusions was less than $25 \mu\text{m}$. At the next moment, the interparticle distance slightly increased. For more than 3 seconds, the interparticle distance remained almost constant.

Because liquid inclusions were never observed under the conditions described, observations using synthetic inclusions were attempted. To avoid the formation of inclusions other than liquid, a more reducing atmosphere, $\text{Ar} + 3 \text{ pct } \text{H}_2$, gas mixture was employed.

As soon as the iron is molten, numerous liquid inclusions could be observed. Their size varied from a few to $10 \mu\text{m}$ in an earlier stage of the observation as shown in Figure 9. The liquid inclusions often were in a group of inclusions with various sizes. The attraction or agglomeration among the liquid inclusions was rarely observed despite the initially short interparticle distance.

However, when external conditions met—probably the momentum of the surface flow and the movement of other inclusions—some liquid inclusions could meet and agglomerate, resulting in a similar spherical shape. Figure 10 shows these interactions of the liquid inclusions. Note that L and S stand for liquid inclusion and solid inclusion, respectively. As mentioned in the sample preparation section, the liquid inclusions are calcium aluminate and the solid inclusions are alumina. At the initial stage, inclusion L1 consists of five liquid inclusions, which are in contact with each other, whereas inclusions L2, L3, S1, and S2 exist separately. Figure 10 shows that L1, L2, and L3 keep almost the same distance with each other, although the distances between them are small. In inclusion L1, the agglomerations of small inclusions into a larger one in contact took place

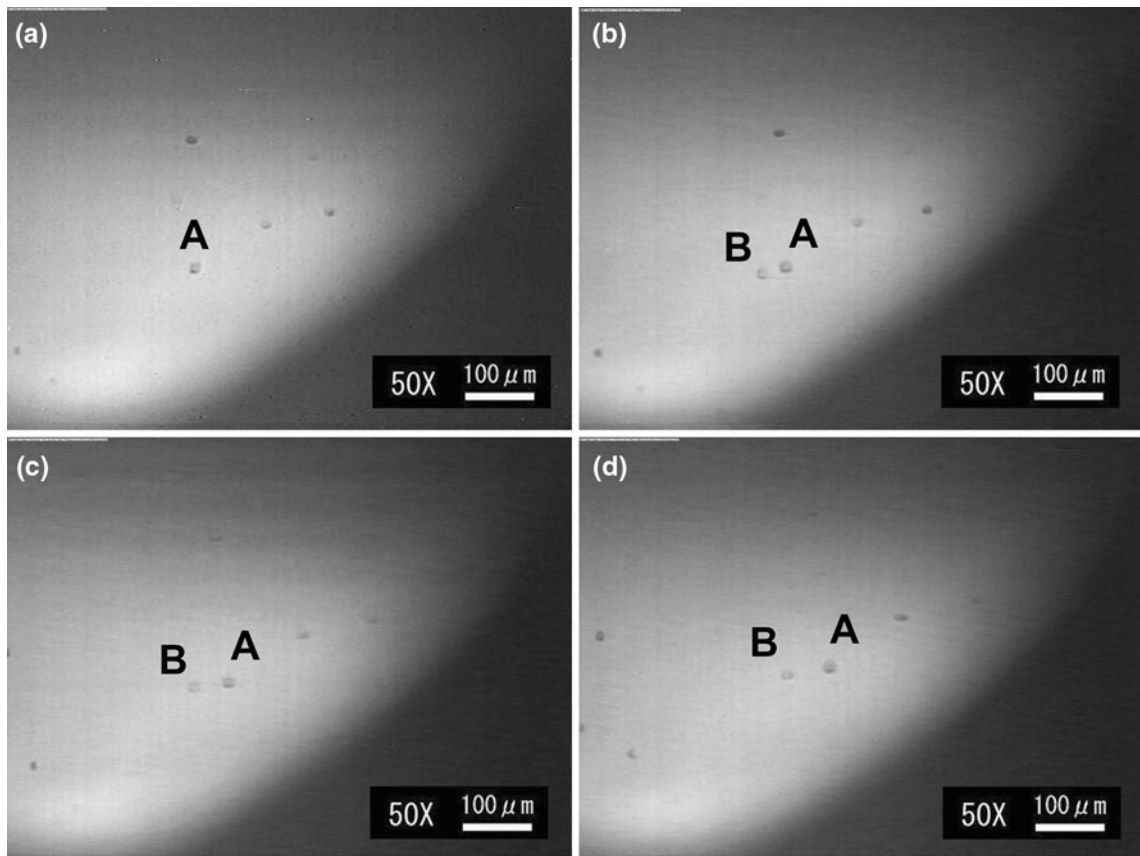


Fig. 8—Images from the CSLM, showing a pair of $\text{CaO } 2\text{Al}_2\text{O}_3$ inclusions keeping their distance from each other: (a) $t = 0.0$ s, (b) $t = 1.0$ s, (c) $t = 3.0$ s, and (d) $t = 5.0$ s.

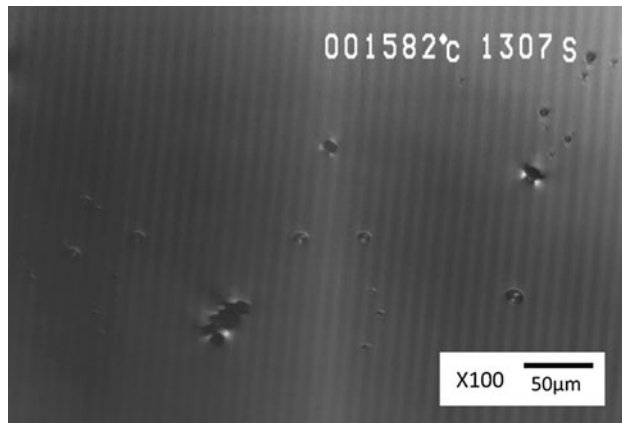


Fig. 9—Images showing numerous liquid inclusions just after melting.

at 0.1 and 0.5 seconds. Note that the merging process of small liquid inclusions is not a result of attraction as in the case of alumina. The liquid inclusions met each other probably because of the momentum of the surface flow, as no acceleration towards each other was noted. The attraction followed by agglomeration of alumina inclusions was observed again in this sample. As shown in Figure 10, inclusions S1 and S2 approached each other and merged into S1 + 2 at $t = 0.2$ s.

When the agglomerated solid inclusion became large enough, it was observed that even a part of the liquid inclusions agglomerated with the alumina inclusions. Figure 11 shows the interactions between liquid and solid inclusions. At $t = 0.0$ seconds, inclusions S1 and L1 approach each other with time. Even in this case, the approaching was not because of the attractive interaction but the surface flow because no acceleration was involved. The fact that several solid and liquid inclusion pairs kept constant small distances (about $20 \mu\text{m}$) with time would be another evidence of the absence of attraction between liquid and solid. At $t = 0.7$ s, inclusions S1 and L1 collided and agglomerated into S1 + L1. After the agglomeration, the spherical shape of the liquid inclusions immediately disappeared and inclusion S1 + L1 became an irregular shape. It is reasonable to expect that the agglomeration of S1 and L1 resulted in a chemical reaction between the two phases. The irregular shape indicated that the reaction product is solid—likely a calcium aluminate with high Al_2O_3 content. Similarly, another irregular inclusion appeared probably because of the agglomeration of inclusion S2 and L4. It should be mentioned that, in the early stage of the observation, the agglomeration and growth of the alumina inclusion were dominant because of the strong, long-range attraction between them. After a while, the collision and the agglomeration of liquid inclusions and solid inclusions were occasionally

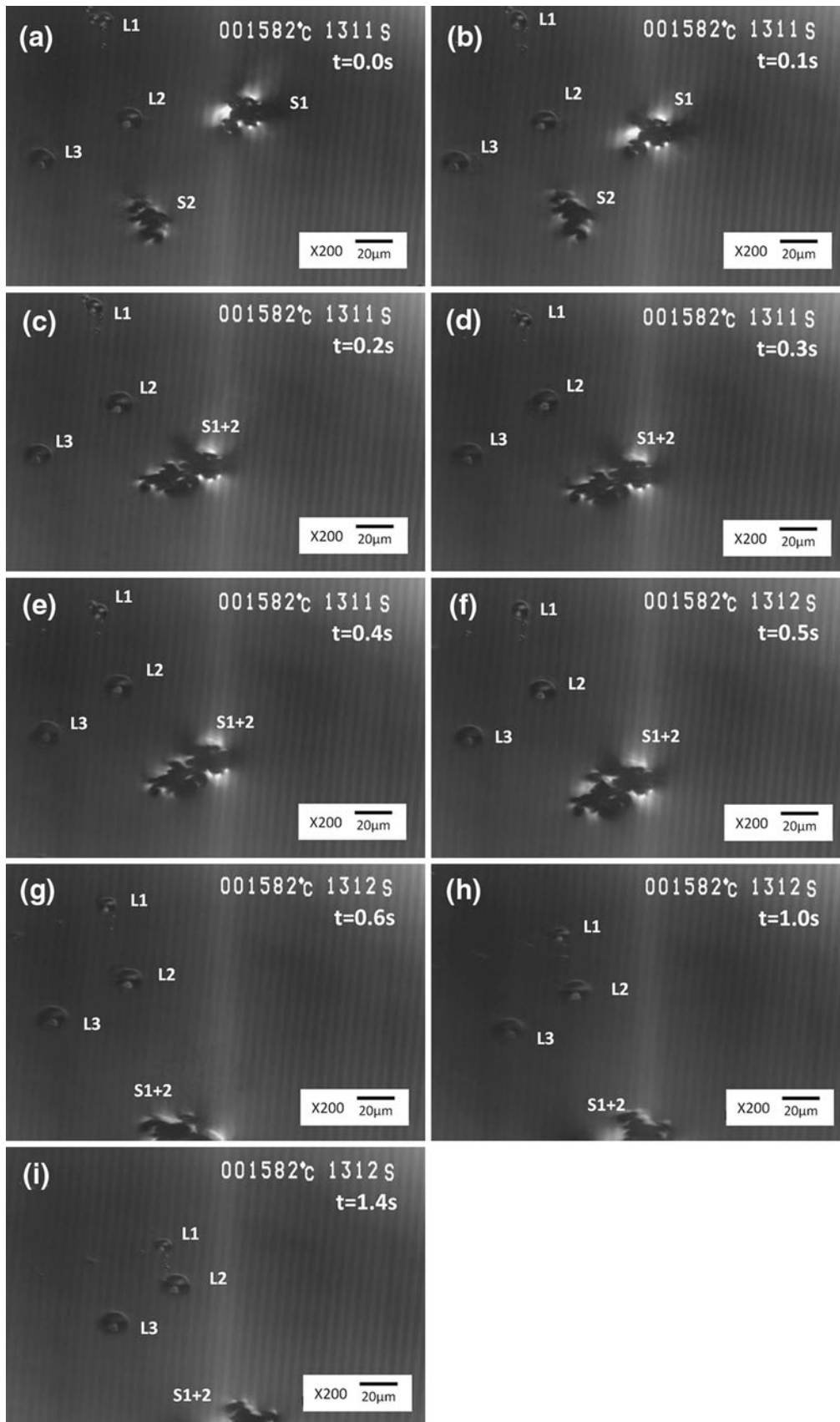


Fig. 10—Images showing the interactions among liquid inclusions (L1 through L3) and solid inclusions (S1, S2), respectively.

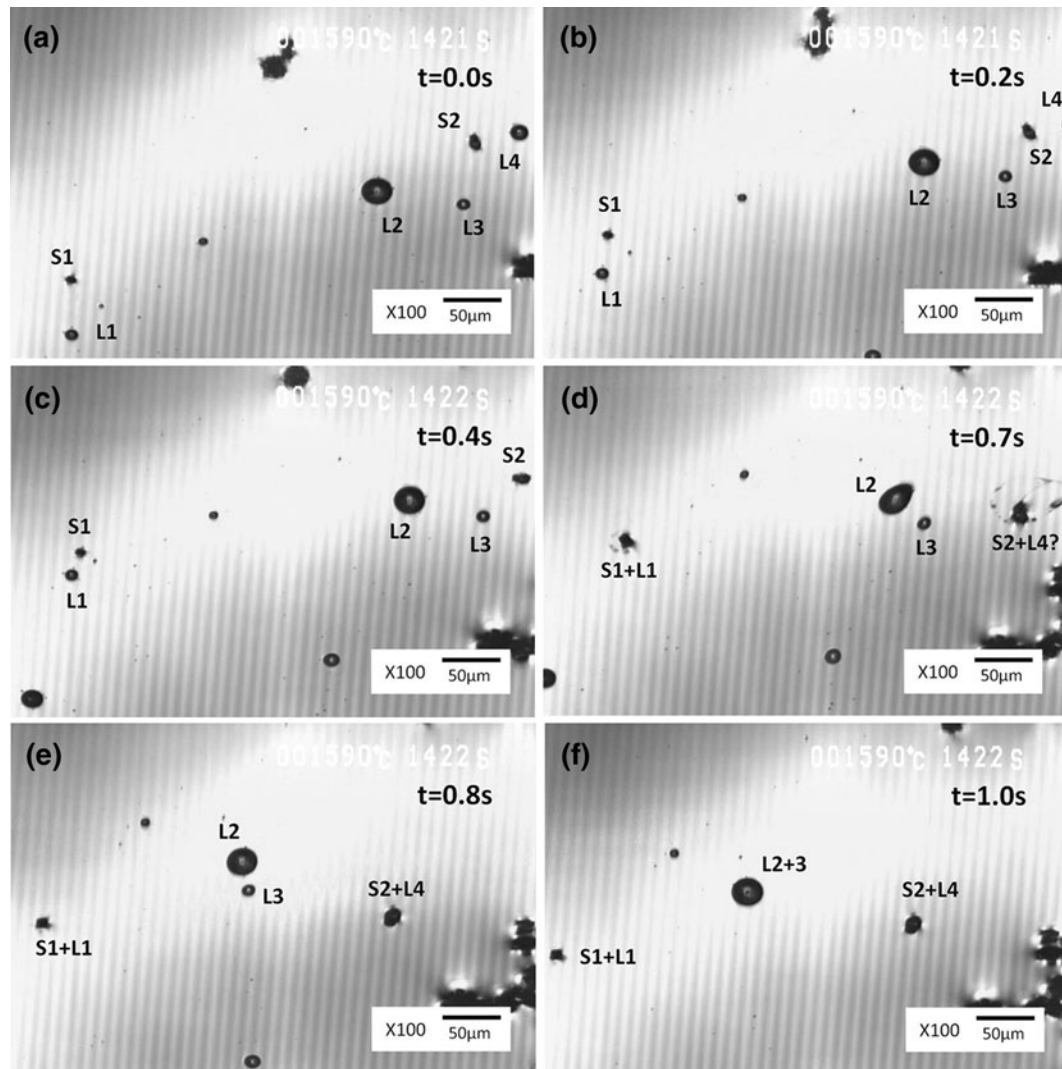


Fig. 11—Images showing the interactions among liquid inclusions and solid inclusions, respectively.

observed possibly because of the increasing probability of inclusion collision with the size of the alumina inclusions.

It must be pointed out that the merging of S1 and L1 as well as S2 and L4 were different from the attraction process observed for alumina inclusions (Figure 4). In the case of alumina inclusions, a clear acceleration was noticed when two particles begin to attract each other (Figure 4). However, no acceleration was ever observed between any of the liquid inclusions as well as between alumina and liquid inclusions. Moreover, the merging shown in Figure 11 is rarely observed. The present result indicates that, although agglomeration could take place between liquid inclusions as well as between alumina and liquid inclusions when they meet occasionally, their meetings are not caused by a mutual attraction process but by external help-like surface flow.

It should be mentioned that, although the agglomeration of liquid calcium aluminate inclusions as well as alumina and liquid calcium aluminate inclusion does not play an important role in ladle treatment, it would need great attention during casting. In ladle treatment, the

meeting probability of these types of inclusions is low because it needs an external force. However, the meeting probability would be high when the liquid steel flows through a narrow orifice as in the case of casting. The frequent meetings of these types of inclusions would result in clogging.

A strong movement on the surface around inclusion S2 + L4 was observed. As a result of the agglomeration, other inclusions around S2 + L4 were pushed away from inclusion S2 + L4. In fact, this phenomenon was observed often, and careful observation revealed that the pushing effect was caused not only by the rupture of the liquid inclusion. A sudden change of the interfacial tension between an inclusion and the liquid steel could be one reason. However, this phenomenon needs more detailed investigation in the future.

C. Interactions Between Inclusion Particles on Liquid–Steel Surface

Obviously, the attractive interaction and the agglomerating tendency of spinel and calcium aluminate

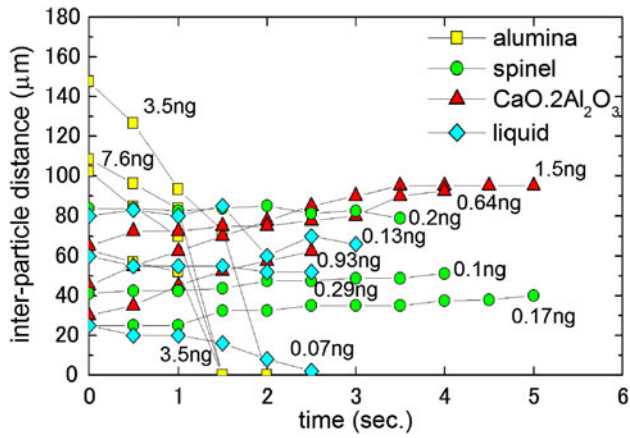


Fig. 12—Interparticle distance of various types of inclusions as functions of time.

inclusions (solid or liquid) were not as significant as those of the alumina inclusions. Figure 12 presents the interparticle distances as functions of time for different types of inclusions. The value marked for each line stands for the geometric average mass of the pair of inclusions observed. The great difference in the agglomeration behavior among the alumina inclusions, the spinel, $\text{CaO} \cdot 2\text{Al}_2\text{O}_3$, and the liquid inclusions is illustrated by the figure. To answer the question of why only the alumina inclusions show strong agglomeration behavior, the origin of the attractive force needs to be examined.

At first, it may be considered that the mass attractive force is responsible for the attraction between inclusions. The mass attractive force can be calculated for various inclusions including alumina inclusions for comparison. Theoretically, the gravitation force $F_{\text{gravitation}}$ is proportional to the masses M_1 and M_2 of the moving objects and the reciprocal of the square of the distance R between them, which is expressed as follows:

$$F_{\text{gravitation}} \propto \frac{M_1 \times M_2}{R^2} \quad [1]$$

For instance, inclusions C and D in Figure 4 did not approach each other, whereas inclusions A and B were attracting and agglomerating. A simple calculation with the initial interparticle distances and sizes obtained from several image analyses indicates that the attractive force between A and B is almost four times greater than that between C and D. The big difference in the mass attractive force is in accordance with the difference in attraction between the two pairs of inclusions. It is reasonable to believe that the mass attractive force is one dominating factor in the attraction of the alumina inclusions.

To examine whether the attractive force is the only major force leading to the impact and agglomeration of the inclusions, the values of $\frac{M_1 \times M_2}{R^2}$ for different pairs of alumina, spinel, $\text{CaO} \cdot 2\text{Al}_2\text{O}_3$, and liquid inclusions are evaluated based on the CSLM observation. However,

Table V. Estimated $\frac{\bar{M}^2}{R^2}$ (Relative Gravitation Force) of the Inclusions Shown in Figure 8

	\bar{M} (kg)	R (m)	$\frac{\bar{M}^2}{R^2}$
Alumina	7.6×10^{-12}	1.0×10^{-4}	5.4×10^{-15}
	3.5×10^{-12}	1.0×10^{-4}	1.2×10^{-15}
$\text{MgO} \cdot \text{Al}_2\text{O}_3$	3.5×10^{-12}	6.3×10^{-5}	3.1×10^{-15}
	2.1×10^{-13}	8.4×10^{-5}	6.3×10^{-18}
$\text{CaO} \cdot 2\text{Al}_2\text{O}_3$	1.0×10^{-13}	4.1×10^{-5}	6.4×10^{-18}
	1.7×10^{-13}	2.5×10^{-5}	4.8×10^{-17}
Liquid inclusions	1.5×10^{-12}	4.5×10^{-5}	1.1×10^{-15}
	6.4×10^{-13}	6.5×10^{-5}	9.6×10^{-17}
Liquid inclusions	9.3×10^{-13}	3.0×10^{-5}	9.5×10^{-16}
	1.3×10^{-13}	8.0×10^{-5}	2.7×10^{-18}
	2.9×10^{-13}	6.0×10^{-5}	2.3×10^{-17}
	7.1×10^{-14}	2.5×10^{-5}	8.0×10^{-18}

the assumption that the inclusions are spheres with the diameters as observed under the microscope cannot be accepted for liquid inclusions. A liquid inclusion on the liquid steel surface is expected to have a lens shape. To estimate the volume of a liquid inclusion with observed diameter r , it was assumed that liquid steel surface keeps its flatness even at the three-phase (gas-inclusion-liquid steel) contact. Additionally, the contact angle and the density difference between calcium aluminate liquid slag (50 mass pct $\text{CaO} \cdot \text{Al}_2\text{O}_3$) and liquid steel (contact angle = 58° ^[28] and $\rho_{\text{Fe}} = 7.0 \text{ g/cm}^3$, $\rho_{\text{CaO} \cdot \text{Al}_2\text{O}_3 \text{ slag}} = 2.7 \text{ g/cm}^3$) were employed. From the equilibrium between the gravitation and the buoyant force, the apparent contact angle and the approximated volume of the liquid inclusions are 35° and $0.266 r^3$, respectively. Thus, the mass of the liquid inclusions was calculated using this expression. The results are presented in Table V. Although spinel and liquid inclusions exhibit lower attractive forces because of their smaller weights, the attractive forces between the $\text{CaO} \cdot 2\text{Al}_2\text{O}_3$ inclusions and between alumina inclusions lay at the same level. However, Figure 11 indicates that both spinel and $\text{CaO} \cdot 2\text{Al}_2\text{O}_3$ inclusions remain separated without attracting, despite shorter initial distances. The comparable mass attractive forces between $\text{CaO} \cdot 2\text{Al}_2\text{O}_3$ as well as between alumina inclusions and their different behaviors in attraction suggest that the mass attractive force is not the only dominating force for attraction and agglomeration.

The capillary effect has been considered as another attractive force.^[18,19] When two particles floating on a liquid surface in a mutually nonwetting condition are getting close to each other, the inner surface between the two particles would be lower than the outer surface because of the capillary effect. According to the theory, the capillary pressure caused by the height difference drives the two particles to approach each other. The following approximated expression for the attraction force has been suggested^[23]:

$$F = 0.5g(\rho_L - \rho_G)w\Delta h^2 \quad [2]$$

where g is the gravity acceleration, w is the horizontal diameter of the particle, and ρ_L and ρ_G are the densities of the liquid and gas. Δh in Eq. [2] stands for the

Table VI. Estimated $-\frac{\cos\theta}{R}$ of the Inclusions Shown in Figure 8

	θ (deg)	R (m)	$-\frac{\cos\theta}{R}$
Alumina	135	1.0×10^{-4}	7071
		1.0×10^{-4}	7071
MgO Al ₂ O ₃	134	6.3×10^{-5}	11,224
		8.4×10^{-5}	8270
		4.1×10^{-5}	16,943
CaO 2Al ₂ O ₃	120	2.5×10^{-5}	27,786
		4.5×10^{-5}	11,111
		6.5×10^{-5}	7692
		3.0×10^{-5}	16,667

equilibrium height difference between the surfaces inside and outside of the particles and is expressed as follows:

$$\Delta h = \frac{2\gamma \cos\theta}{g(\rho_L - \rho_G)R} \quad [3]$$

where γ , θ , and R are the surface tension of the liquid, the contact angle of the particles on the liquid, and the distance between the two particles, respectively. The capillary pressure is strongly dependent on the height difference Δh as it increases to a power of two.

The contact angles of alumina, spinel, and CaO 2Al₂O₃ inclusions with liquid iron at 1873 K (1600 °C) have been reported to be 135 deg, 134 deg, and 120 deg, respectively.^[21,28,29] An examination of Eqs. [2] and [3] shows that only the value of $\frac{\cos\theta}{R}$ depends on the type of inclusions, whereas the other variables are independent of the type. A comparison of the values of $\frac{\cos\theta}{R}$ for different pairs of inclusions would reveal the function of the capillary effect. The calculated values of $\frac{\cos\theta}{R}$ are listed in Table VI, which shows that the values of $\frac{\cos\theta}{R}$ of different types of inclusions are at the same level.

The similarity of the $\frac{\cos\theta}{R}$ values as well as the different behaviors of spinel and CaO Al₂O₃ inclusions from that of alumina inclusions with respect to attraction and agglomeration strongly suggest that capillary force is not the major force leading to the agglomeration of the inclusions. Moreover, because compared with other solid inclusions, liquid calcium aluminate inclusion is known to have a contact angle less than 90 deg with liquid steel,^[28] the inner surface between a pair of inclusions is expected to be raised when the interparticle distance is sufficiently small. Then, the capillary pressure will cause repulsion between inclusions, which is not at all consistent with the CSLM observation in the present study.

It also is noted that the capillary force can be applied to the attractive interaction of inclusions only at the liquid metal surface or the slag-metal interface. Therefore, a comparison of the results of CSLM with the industrial data is absolutely essential to obtain a better grip of this aspect.

D. Comparison of the Results of CSLM with the Industrial Finding

As shown in Table III and Figure 3, no indication of attachment or agglomeration of inclusions except

alumina was observed. The agglomeration of alumina inclusions has been a topic for many researchers. For the sake of brevity, no intensive discussion about alumina inclusions will be given. However, it is still worthwhile to mention that the steel samples taken during deoxidation at Uddeholm Tooling AB contained alumina clusters (Figure 3^[27]). The existence of Al₂O₃ clusters even in the bulk steel sample may be in accordance with the behavior of alumina inclusions on the liquid steel surface observed by CSLM in the present study.

At least some attachments of spinel inclusions would have been found in the industrial samples if the inclusions had had a tendency to attract and agglomerate in the ladle. The examination of almost 8000 spinel inclusions would provide strong evidence for the absence of agglomeration of spinel particles. This industrial finding also is supported by the CSLM results.

Inclusions of type 2, 4, 6, 7, and 8 in Table II all have a liquid oxide phase in contact with liquid steel. According to the present CSLM observations, single-phase liquid inclusions (type 7) do not have attractive tendency, although they meet occasionally by external force. As revealed by the CSLM observation, part of the liquid inclusions undergo agglomeration by the external factors, such as surface flow, whereas the rest are likely to remain separated. These findings agree well with the previous research.^[24]

It was also observed that, after the collision between the liquid inclusion and the irregular inclusion (alumina in the most cases), the liquid inclusion rapidly turns into a solid inclusion. The absence of a solid calcium aluminate inclusion in the industrial steel samples could be explained by the rapid removal of alumina clusters in the process. However, single alumina particles do exist in some ladles in other steel plants where a different deoxidation practice is employed. In such cases, the formation of some solid calcium aluminate inclusions could be a result of the reaction between a solid alumina inclusion and liquid calcium aluminate inclusion.

The formation of types 6 and 8 inclusions hardly depends on the agglomeration. It is expected that the complex inclusions are probably formed by the interfacial reaction between solid inclusions and liquid steel.^[21]

The mutual conformity of the industrial data and the *in situ* observation by the laser microscope suggests that, although the growth of alumina inclusions is mostly dependent on self-attraction, the physical growth by agglomeration of the other types of inclusions has much less importance for the inclusion control in ladle treatment.

IV. SUMMARY

To obtain a better understanding of the growth of nonmetallic inclusions in liquid steel, the behavior of the inclusions was studied. Numerous steel samples were taken at different stages of ladle treatment. The phases and morphology of the different types of inclusions were obtained by SEM and LOM. In total, about 30000 inclusions were examined. No indication of any

attachment and agglomeration were observed in the case of inclusions of spinel or inclusions that have a liquid oxide solution (calcium aluminate) phase in contact with steel. Their behavior was contradictory with that of alumina inclusions, which attracted each other and agglomerated easily.

To obtain insight of the industrial results, the behavior of different types of inclusions was examined using a CSLM. Alumina particles attracted each other and agglomerated, as reported in the literature. However, spinel inclusions and solid calcium aluminate inclusions did not show any sign of attraction or agglomeration. The mass attractive force and capillary force were estimated for different types of inclusions. A comparison of the calculated results and the experimental observation showed that the mass attractive force is one but not the only dominating force leading to attraction and agglomeration. The comparison also indicated that the argument that the capillary force resulting in the agglomeration would require reconsideration.

ACKNOWLEDGMENTS

The authors are thankful to Dr.-Ing. H.P. Heller and Dr.-Ing. A. Franke, Institute of Iron and Steel Technology, Freiberg University of Mining and Technology, for their helps in the analyses. Financial support for this work provided by Uddeholm Tooling AB is gratefully acknowledged.

REFERENCES

1. Y. Miki, H. Kataoka, T. Sakuraya, and T. Fujii: *Tetsu-to-Hagane*, 1992, vol. 78, pp. 431–38.
2. Y. Sahai and T. Emi: *ISIJ Int.*, 1996, vol. 36, pp. 1166–73.
3. H. Tozawa, Y. Kato, K. Sorimachi, and T. Nakanishi: *ISIJ Int.*, 1999, vol. 39, pp. 426–34.
4. U. Lindborg and K. Torsell: *Trans. TMS-AIME*, 1968, vol. 242, pp. 94–102.
5. P. Kosakevitch and M. Olette: *Iron Steel Inst.*, 1972, vol. 134, pp. 42–49.
6. P. Kosakevitch and M. Olette: *Miner. Met. Rev.*, 1971, vol. 68, pp. 635–46.
7. G. Ebnet and K. Rüttiger: *Arch. Eisenhüttenw.*, 1976, vol. 47, pp. 277–81.
8. G. Ebnet and K. Rüttiger: *Arch. Eisenhüttenw.*, 1976, vol. 47, pp. 339–43.
9. H. Chikama, H. Shibata, T. Emi, and M. Suzuki: *Mater. Trans.*, 1996, vol. 37, pp. 620–26.
10. H. Shibata, Y. Arai, M. Suzuki, and T. Emi: *Metall. Mater. Trans. B*, 2000, vol. 31B, pp. 981–91.
11. H. Shibata, H. Yin, S. Yoshinaga, T. Emi, and M. Suzuki: *ISIJ Int.*, 1998, vol. 38, pp. 149–56.
12. H. Yin, T. Emi, and H. Shibata: *Acta Mater.*, 1998, vol. 47, pp. 794–801.
13. K.W. Yi, C. Tse, J.-H. Park, M. Valdez, A.W. Cramb, and S. Sridhar: *Scand. J. Metall.*, 2003, vol. 32, pp. 177–84.
14. S. Sridhar and A.W. Cramb: *Metall. Mater. Trans. B*, 2000, vol. 31B, pp. 406–10.
15. M. Valdez, K. Prepakorn, A.W. Cramb, and S. Sridhar: *Steel Res. Int.*, 2001, vol. 72, pp. 291–97.
16. B.J. Monaghan, L. Cen, and J. Sorbe: *Ironmaking Steelmaking*, 2005, vol. 32, pp. 258–64.
17. Y. Li and R.J. Fruehan: *Metall. Mater. Trans. B*, 2001, vol. 32B, pp. 1203–05.
18. Y. Wang, M. Valdez, and S. Sridhar: *Metall. Mater. Trans. B*, 2002, vol. 33B, pp. 625–32.
19. M. Valdez, Y. Wang, and S. Sridhar: *Steel Res. Int.*, 2004, vol. 75, pp. 247–56.
20. C. Orrling, S. Sridhar, and A.W. Cramb: *ISIJ Int.*, 2000, vol. 40, pp. 877–85.
21. P. Misra, V. Chevrier, S. Sridhar, and A.W. Cramb: *Metall. Mater. Trans. B*, 2000, vol. 31B, pp. 1135–39.
22. B. Colletti, S. Vantilt, B. Blanpain, and S. Sridhar: *Metall. Mater. Trans. B*, 2003, vol. 34B, pp. 533–38.
23. H. Yin, H. Shibata, T. Emi, and M. Suzuki: *ISIJ Int.*, 1997, vol. 37, pp. 936–45.
24. H. Yin, H. Shibata, T. Emi, and M. Suzuki: *ISIJ Int.*, 1997, vol. 37, pp. 946–55.
25. Y. Kang, M. Nzotta, and D. Sichen: *Steel Grips*, 2007, vol. 5, pp. 18–34.
26. N. Tripathi and D. Sichen: *Ironmaking Steelmaking*, 2006, vol. 33, pp. 213–22.
27. K. Beskow, J. Jia, C.H.P. Lupis, and D. Sichen: *Ironmaking Steelmaking*, 2002, vol. 29, pp. 427–35.
28. A.W. Cramb and I. Jimbo: *Ironmaking Steelmaking*, 1989, vol. 16, pp. 43–55.
29. N. Shinozaki, Y. Takahashi, and K. Mukai: *Tetsu-to-Hagane*, 1994, vol. 80, pp. 748–53.